ISSN 2616-5775 Vol. 9, Issue 1: 56-62, DOI: 10.25236/AJCIS.2026.090107

Dual-Stage Geometric Calibration for Artifact Suppression in Cone-Beam CT

Yulong Zhang[1,+], Zhen Zhang[2,+,*], Jianqiang Mei[1]

[1]*School of Electronic Engineering, Tianjin University of Technology and Education, Tianjin, 300222, China*
[2]*Nanjing Chenguang Group Co., Ltd., Nanjing, 210006, China*
[+]*These authors contributed equally to this work.*
[*]*Corresponding author:759272431@qq.com*

Abstract: *To address artifacts and shape deviations in cone-beam CT (CBCT) caused by geometric misalignments, this study proposes a phantom-free two-stage calibration scheme. Detector pre-correction is first performed to lay a foundation for subsequent rotation-axis optimization, with the latter leveraging a Sharpness-Maximized Matching (SMM) strategy as the core. Specifically, detector pre-correction is achieved via symmetry-aware SIFT matching, adaptive sampling, and doubly-weighted optimization to estimate the detector's horizontal offset. For rotation-axis optimization, an improved evaluation function is introduced under the SMM framework, and the optimal horizontal offset of the rotation axis is determined through iterative reconstruction within a predefined search range. Experiments on a set of industrial workpiece projection data demonstrate that the proposed two-stage scheme effectively eliminates artifacts, outperforms SAM and WAC in both image sharpness and measurement accuracy, and enables high-precision non-destructive testing without relying on dedicated phantoms.*

Keywords: *Cone-Beam Computed Tomography, Geometric Calibration, Rotation-Axis Correction, SIFT Feature Matching*

1. Introduction

Industrial Computed Tomography (ICT)[1] has emerged as a crucial non-destructive testing (NDT)[2] technology in modern manufacturing. It enables volumetric inspection of complex parts, providing detailed internal structural information. By utilizing X-ray penetration and digital reconstruction[3] algorithms, ICT can generate three-dimensional visualizations of the internal microstructures of workpieces. This technology has become an essential tool for quality control in industries such as aerospace, automotive, and electronics. Industrial CT (ICT) can perform volume inspection on complex components, but subtle geometric deviations, especially the lateral offset of the rotation axis, can cause circular/arc-shaped artifacts[4] and shape deviations[5], thereby reducing image quality and dimensional accuracy. In CBCT systems, the coupling effect of detector offset[6] and rotation axis offset[7-8] can exacerbate this problem at high magnification, so robust calibration is particularly important in production environments.

The existing technical solutions are mainly divided into three categories: (i) symmetry center estimation algorithms[9] (such as sine wave center method, relative angle method, curve fitting method); (ii) Correlation/optimization algorithms (such as SAM[10], WAC[11]); (iii) Geometric/phantom calibration techniques[12] (using precision spheres or plates). The symmetry-based methods are sensitive to noise and auxiliary structures (e.g., workbenches and fixtures); correlation-based methods may fail when processing periodic textures; phantom-based calibration not only incurs high costs but also suffers from inherent tolerance errors of the calibration phantom.

This study presents an innovative two-stage calibration scheme. The first stage focuses on estimating and pre-correcting the detector lateral shift. By leveraging the symmetry of projections, we employ a combination of the Scale-Invariant Feature Transform (SIFT[13]), adaptive sampling, and doubly-weighted optimization. This approach allows for a more accurate determination of the detector shift, effectively decoupling it from the rotation-axis offset. In the second stage, we optimize the rotation-axis offset by maximizing the sharpness of the reconstructed slices. We use a Scharr-based center-Region of Interest (ROI) score to precisely lock the remaining axis offset. This two-stage approach not only

ISSN 2616-5775 Vol. 9, Issue 1: 56-62, DOI: 10.25236/AJCIS.2026.090107

decouples the detector horizontal offset from the rotation-axis horizontal offset (the two primary geometric error sources) but also significantly improves the robustness of the calibration process. Additionally, it eliminates the need for dedicated calibration phantoms, making it more cost-effective and adaptable to various industrial applications.

The remaining structure of this article is arranged as follows: Section 2 introduces the proposed method and elaborates on the detector pre correction method and the rotation axis offset correction method in detail. Section 3 presents the complete process and results of the experiment, including quantitative and qualitative evaluations. Finally, Section 4 summarizes the contributions and findings of this article.

2. Methodology

In this section, we first introduce the overall architecture of the proposed method. Subsequently, we provided detailed descriptions of detector pre calibration and rotation axis calibration.

2.1 Overview architecture

The proposed calibration method consists of two main stages. In the first stage, we focus on the pre-correction of the detector. We take advantage of the 180° rotation symmetry of projections in cone-beam CT full-circle scans. By using the Scale-Invariant Feature Transform (SIFT) algorithm, we extract stable feature points from the projection images. Then, an adaptive sampling strategy is applied to optimize the spatial distribution of these feature points. After that, a doubly-weighted optimization based on feature-point response values and direction consistency is carried out to accurately calculate the detector lateral shift. This pre-correction of the detector helps to decouple the influence of detector shift from the rotation-axis offset, providing a more accurate foundation for the subsequent rotation-axis optimization.

In the second stage, we turn to the optimization of the rotation-axis parameters. The sharpness-maximization principle adopted herein is derived from the autofocus mechanism widely used in camera systems—one that has been successfully adapted for X-ray CT geometric calibration[14-15]. This principle is grounded in a straightforward physical observation: when the rotation axis deviates from its ideal position, the projection data fails to align with the geometric constraints of the reconstruction algorithm, leading to blurred edge structures and reduced definition in the reconstructed slices. Conversely, when the rotation axis is accurately calibrated, the edge features of the object are optimally focused in the reconstructed slices, resulting in the highest possible sharpness. To quantify this sharpness, we evaluate the gray value gradients of the reconstructed images—edge regions exhibit steeper gradient changes, which directly translate to a higher sharpness score. We use a Scharr-based center-Region of Interest (ROI) score to evaluate the sharpness of the reconstructed slices. By generating a sequence of candidate offset values within a preset search range and performing iterative reconstruction-evaluation iterations, the optimal rotation-axis offset that maximizes the sharpness of the reconstructed slices can be precisely determined. This two-stage scheme effectively addresses the geometric misalignment issues in CBCT, improving the quality of the reconstructed images.

2.2 Detector Pre-Correction via Symmetry Matching

In cone-beam CT full-circle scans, projections exhibit an inherent 180° rotational symmetry: the projection at angle β is symmetric to that at $\beta+\pi$ about the rotation axis center. Any deviation from this symmetry indicates a detector shift, forming the theoretical basis for horizontal shift correction. As shown in Figure 1, the correction workflow consists of SIFT feature extraction and shift calculation/optimization. By analysing the discrepancy between ideal symmetric and actual projection positions, the detector shift is estimated and corrected, laying a foundation for accurate subsequent rotation-axis calibration.

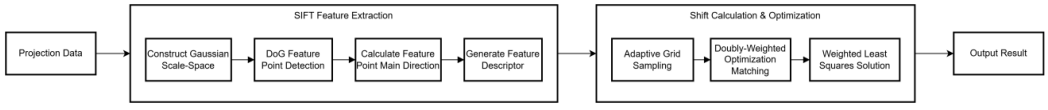

Figure 1: Flowchart of detector shift correction.

The SIFT algorithm is fundamental for extracting stable feature points from projection images to calculate detector shift, with a sequential process ensuring rotation invariance and scale robustness. First, multi-scale space is constructed by convolving the projection image $I(x,y)$ with 2D Gaussian kernels

ISSN 2616-5775 Vol. 9, Issue 1: 56-62, DOI: 10.25236/AJCIS.2026.090107

$G(x,y,\sigma)$, generating the scale-space image:

$$L(x,y,\sigma) = G(x,y,\sigma) * I(x,y) \tag{1}$$

This creates a series of blurred images that enable the detection of features stable across different scales.

Subsequently, using Difference of Gaussian (DoG) operator to detect extremum points (Eq. (2)), which correspond to stable edge/corner structures in projections:

$$D(x,y,\sigma)=[G(x,y,k\sigma)-G(x,y,\sigma)]*I(x,y) \tag{2}$$

To achieve rotational invariance, the gradient direction of pixels around each feature point is calculated (Eq. (3)), and a gradient direction histogram determines the main feature direction, eliminating projection rotation errors in matching:

$$\theta(x,y) = atan2\big(L(x,y+1) - L(x,y-1), L(x+1,y) - L(x-1,y)\big) \tag{3}$$

A rotation-invariant feature vector $F = \left[h_1^{(1,1)}, \ldots, h_8^{(4,4)}\right]^T$ is then generated, enabling precise matching of homologous feature points across projections for shift calculation.

To enhance shift calculation accuracy, an integrated strategy of adaptive sampling and doubly-weighted optimization is adopted. In adaptive sampling, the image is divided into a 3×3 grid (ensuring at least one feature point per grid), and a mixed-scoring system weights feature response values and coordinate ratios to filter redundant points while preserving key edge features.

For doubly-weighted optimization, a weighted mechanism is applied to matching feature point pairs (p_i, p_j) to avoid equal treatment of feature points in traditional methods. The weight w_{ij} is calculated as Eq. (4):

$$w_{ij} = \frac{exp\left(\alpha \cdot R_i + \beta \cdot cos\left(\theta_i - \theta_j\right)\right)}{\sum_{k=1}^{N} exp\left(\alpha \cdot R_j + \beta \cdot cos\left(\theta_j - \theta_j'\right)\right)} \tag{4}$$

Where R is the feature response value, θ is the feature direction, and (α, β) are adjustable parameters. Pairs with higher responses and consistent directions receive greater weights.

Subsequently, to ensure that these weighted feature pairs contribute proportionally to the displacement estimate, the weights w_{ij} from Eq.(4) are used to construct a weighted least-squares objective function $J(\Delta x)$. This function is minimized via gradient descent to obtain the optimal detector shift Δx^*. In this context, w_i denotes the weight w_{ij} corresponding to the i-th matched point pair (p_i, p_j)

$$J(\Delta x) = \sum_{i=1}^{N} w_i \cdot \left[\left(x_1^{(i)} - x_2^{(i)}\right) - \Delta x\right]^2 \tag{5}$$

Where $x_1^{(i)}$ and $x_2^{(i)}$ are horizontal coordinates of matching point pairs.

2.3 Rotation-Axis Optimization Method Based on Sharpness Maximization

The rotation-axis optimization method based on sharpness maximization is fundamentally grounded in the physical correlation between geometric alignment accuracy and image fidelity. Conceptually analogous to the passive autofocus mechanism in optical systems, this principle has been customized and enhanced to suit the volumetric imaging characteristics of CT. Unlike traditional methods that rely on projection symmetry or dedicated phantoms, the sharpness maximization approach enables phantom-free calibration by leveraging the intrinsic structural information of the measured object itself.

To achieve robust quantification of slice sharpness, this study proposes an improved sharpness evaluation function, addressing the limitations of gradient-based metrics (e.g., summation methods using the Sobel operator) in noise suppression and edge sensitivity. This function integrates three core modules: Scharr gradient calculation for high-precision edge detection, bilateral filtering for noise reduction, and adaptive spatial weighting to emphasize the Region of Interest (ROI). The mathematical expression of the improved sharpness score is defined as:

ISSN 2616-5775 Vol. 9, Issue 1: 56-62, DOI: 10.25236/AJCIS.2026.090107

$$S_{\text{enhanced}}(I) = \sum_{x,y\in\Omega} \| \nabla I_{\text{Scharr}}(x,y) \|_2^2 \cdot W_{\text{adaptive}}(x,y) \cdot W_{\text{bilateral}}(x,y) \quad (6)$$

Where: Ω denotes the entire slice domain; $\nabla I_{\text{Scharr}}(x,y) = \left[\nabla_x I_{\text{Scharr}}(x,y), \nabla_y I_{\text{Scharr}}(x,y)\right]^T$ represents the gradient vector computed using the 3×3 Scharr operator. Compared with the Sobel operator, this operator exhibits superior frequency response characteristics and noise resilience; $W_{\text{adaptive}}(x,y)$ is an adaptive spatial weight mask that assigns higher weights to the central ROI (with a size of $L \times L$), where $L = m \cdot w/\sqrt{2}$, w is the slice width, and m is the margin factor to mitigate the interference of edge noise; $W_{\text{bilateral}}$ accounts for the edge-preserving denoising effect of bilateral filtering, with parameters set to d =9, σ_{color} =0.2, σ_{space} =15, achieving a balance between noise suppression and edge preservation. The asymmetric kernel design of the Scharr operator enhances sensitivity to subtle edge variations, which constitutes a critical technical foundation for subsequent rotation-axis optimization: this enhanced sensitivity enables reliable detection of small rotation-axis offsets (sub-pixel to millimetre scale) in high-magnification scans, a capability that traditional gradient-based metrics struggle to achieve.

To validate the effectiveness of the proposed improved sharpness evaluation function, during the rotation-axis offset calculation process, we compared and analysed the sharpness score curve output by this function with that output by the traditional gradient-based metric (i.e., the Sobel operator-based summation method). The projection data parameters are specified as follows: image dimensions of 700×1000 pixels, source-to-rotation-center distance of 900 mm, rotation-center-to-detector distance of 280 mm, and detector resolution of 0.12 mm × 0.12 mm. Figure 2 presents the sharpness score curves of two evaluation functions (horizontal axis: candidate intervals of the rotation-axis horizontal offset, unit: mm; vertical axes: normalized sharpness scores of the reconstructed slice, with the left axis corresponding to the red curve and the right axis to the blue curve): the blue curve denotes the original Sobel-based metric (traditional gradient-based method), while the red curve represents the improved Scharr-ROI (enhanced) function. Across the offset interval, the enhanced function exhibits a score span of 2.3 (from ~2.5 to ~4.8, relative change rate: 92%), whereas the original metric only has a narrow span of 0.0002 (from ~0.00030 to ~0.00050, relative change rate: 67%). This 37% improvement in the enhanced function's relative change rate makes its score distribution more discriminative, thus enabling precise identification of small rotation-axis offsets.

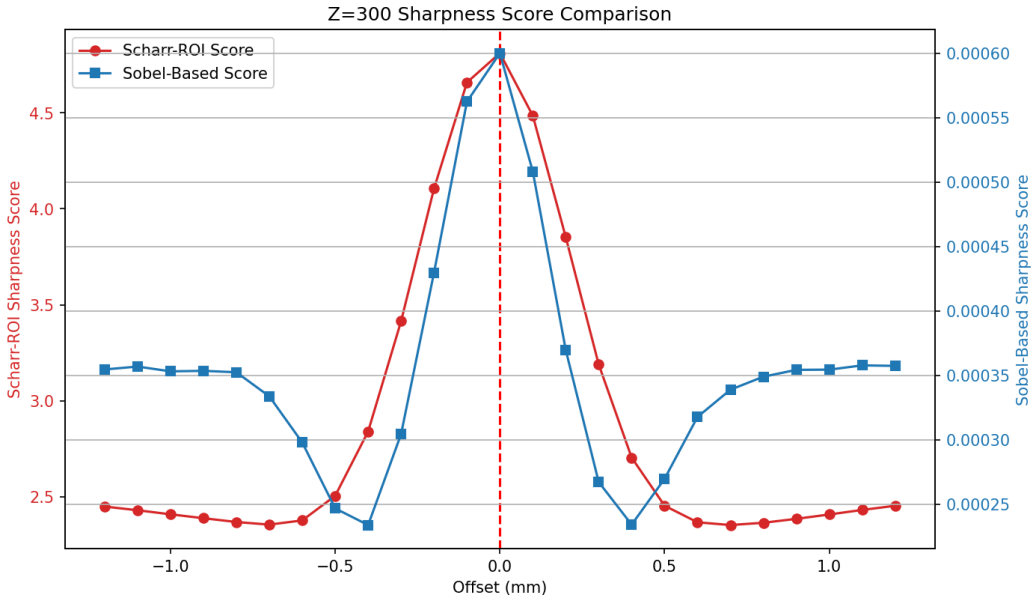

Figure 2: Comparison of sharpness score curves between the pre-improvement (traditional Sobel-based) and post-improvement (Scharr-ROI) evaluation functions

3. Experiments

In this section, we detail the experimental setup and present the results to evaluate the performance of the proposed method. First, we outline the experimental configurations (including hardware and

ISSN 2616-5775 Vol. 9, Issue 1: 56-62, DOI: 10.25236/AJCIS.2026.090107

software) and key implementation details. Next, we provide specifications of the projection data utilized in the experiments. We then introduce the performance metrics adopted for quantitative evaluation, and finally present and analyse the experimental results in depth.

3.1 Hardware environment and software configuration

All experiments were conducted on a computing platform equipped with an AMD Ryzen 7 9800X3D 8-Core Processor and an NVIDIA GeForce RTX 5070 Ti GPU. The algorithm was developed under the Windows operating system and Python 3.13.9 environment. Projection data reconstruction was performed using Astra Toolbox 2.4.0[16], with GPU acceleration enabled via CUDA 12.4.

3.2 Projection Data

This experiment was conducted using an industrial CT imaging system, where the proposed method was applied to correct a set of industrial workpiece projection data, aiming to verify the effectiveness of the method. The acquisition and reconstruction parameters of this projection data are as follows: projection image size of 1024×1024 pixels, distance from the X-ray source to the rotation center of 1350 mm, distance from the rotation center to the detector of 350 mm, 1000 projections, detector pixel size of 0.2 mm, and 720 reconstructed slices. The operating parameters of the X-ray source are: voltage of 180 kV, current of 1.5 mA, and frame rate of 2 fps.

3.3 Experimental results and analysis

To objectively quantify the quality of reconstructed images and verify the effectiveness of the algorithm, three widely used image statistical metrics were selected in this study: mean value, standard deviation, and average gradient. These metrics comprehensively evaluate images from three dimensions: global brightness, noise fluctuation, and edge details. In addition, to verify the feasibility and effectiveness of the proposed algorithm, comparative experiments were conducted between the proposed algorithm and two existing methods. The comparative methods include the SAM method based on statistical average and the WAC method based on weighted average, and the proposed method is denoted as SMM. Table 1 presents the detector horizontal offset measured by SMM's pre-correction module on the selected projection data, along with the quantitative evaluation results of the three calibration methods (SAM, WAC, SMM), including the rotation axis horizontal offset, and the mean value, standard deviation, and average gradient of each image in the reconstructed result comparison diagram.

Table 1: Quantitative evaluation of reconstruction quality for CBCT geometric calibration methods

Detector Horizontal Offset	Rotation Axis Horizontal Offset Correction		Image Quality		
	Correction Method	Measured Result	Mean Value	Standard Deviation	Average Gradient
7.396 mm	SAM	-0.893 mm	113.077	102.695	52.817
	WAC	-1.335 mm	110.347	103.894	50.065
	SMM	-0.527 mm	**105.551**	**104.057**	**52.936**

Figure 3 shows the three-dimensional visualization of the projection data reconstruction results. The workpiece is cylindrical overall with symmetrically distributed hole structures inside, allowing for an intuitive observation of the overall shape of the workpiece and the spatial distribution characteristics of the internal hole structures. Figure 4 shows the results of applying different correction methods to the 686th reconstructed slice. In this experiment, the priority of the correction process is "detector horizontal offset correction → rotation axis horizontal offset correction". This is because detector offset directly leads to overall positional deviation of projection data; if this deviation is not corrected first, subsequent rotation axis offset correction will introduce additional errors. Therefore, all rotation axis correction algorithms are based on projection data after detector correction to ensure a consistent comparison benchmark for different correction methods.

Specifically, the first row of Figure 4 sequentially presents the reconstruction results without any correction, with detector horizontal offset correction (this correction method is used to correct the positional deviation of the detector in the horizontal direction and can reduce reconstruction artifacts caused by detector misalignment), and with rotation axis horizontal offset correction using the SAM algorithm, WAC algorithm, and SMM algorithm (i.e., the rotation axis horizontal offset correction method proposed in this study, which is mainly used to correct the horizontal positional deviation of the

ISSN 2616-5775 Vol. 9, Issue 1: 56-62, DOI: 10.25236/AJCIS.2026.090107

rotation axis during projection data acquisition, and this deviation is one of the core factors leading to blurred contours and artifacts in reconstructed images) on the basis of detector horizontal offset correction. Correspondingly, the second row of Figure 4 shows the magnified images of the Region of Interest (ROI) of each reconstructed image in the first row. The ROI in this study is specifically selected as the contour edge region of the internal structures of the workpiece, as this region is most sensitive to changes in artifacts and structural sharpness and serves as a key region for evaluating correction effects.

A detailed analysis of each correction method's performance is as follows: Figure 4(a) illustrates the uncorrected original reconstruction, which exhibits substantial geometric structural distortion. Focusing on the structural region in the bottom-right corner, prominent edge blurring and morphological deformation are observed—these artifacts critically impair the accurate characterization of the workpiece's internal architecture. Figure 4(b) presents the reconstruction result after detector horizontal offset correction alone. This result shows that edge blurring and morphological distortion are markedly mitigated; however, closer inspection of the magnified ROI (centered on the inner region of the annular structure within the ROI) reveals residual artifacts near the contours, indicating incomplete restoration of structural integrity. Figures 4(c) and (d) depict the results of rotation-axis horizontal offset correction (applied to detector-precorrected data) using the SAM and WAC algorithms, respectively. While these algorithms yield moderate improvements in image quality, residual artifacts persist in the magnified ROI, and the sharpness of structural contours remains suboptimal. Finally, Figure 4(e) shows the reconstruction result obtained by applying the proposed SMM algorithm to detector-precorrected data. Compared with Figures 4(c)–(d), the SMM-corrected image demonstrates significant artifact reduction in both the global view and the targeted ROI: the contours of holes and internal annular structures are sharper, edge details are more distinct, which can more accurately reflect the true structural morphology of the workpiece's interior.

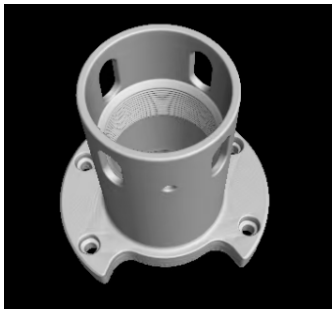

Figure 3: 3D visualization of projection data reconstruction results for the cylindrical workpiece with symmetric internal holes

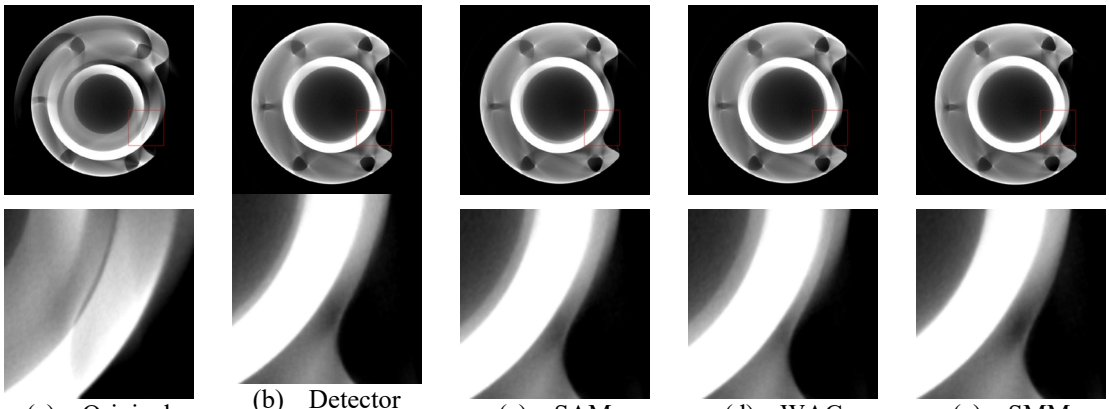

Figure 4: Reconstruction results of the 686th slice under different correction methods

4. Conclusion

To address geometric misalignment-induced artifacts and shape deviations in cone-beam CT (CBCT), this paper proposes a phantom-free two-stage calibration method (SMM): detector pre-correction leverages symmetry-aware SIFT matching, adaptive sampling, and doubly-weighted optimization to accurately estimate horizontal detector offsets, laying a robust foundation for subsequent calibration,

ISSN 2616-5775 Vol. 9, Issue 1: 56-62, DOI: 10.25236/AJCIS.2026.090107

while rotation-axis optimization uses a sharpness-maximization criterion—integrating Scharr edge detection, bilateral filtering, and adaptive ROI weighting—to iteratively determine optimal rotation-axis offsets, outperforming traditional metrics in sensitivity and noise resilience. Experimental results on industrial workpiece data show that for the industrial workpiece projection data, the SMM method calculates the rotation-axis horizontal offset as -0.527 mm; meanwhile, the image quality metrics (mean: 105.551, average gradient: 52.936) of the reconstructed images after calibration using SMM outperform those of the SAM and WAC methods. Specifically, the average gradient of the images processed by SMM is 0.119 and 2.871 higher than that of the images processed by SAM and WAC, respectively. It effectively eliminates artifacts, yields clearer structural contours, and avoids phantom-related costs or tolerances. Limitations include a focus on 2D offsets, so future work will extend to 3D geometric errors and accelerate optimization for real-time industrial inspection. This method enhances CBCT accuracy and cost-effectiveness, supporting high-precision non-destructive testing in manufacturing.

Acknowledgements

This work is supported by Teaching Reform and Quality Construction Research Project of Tianjin University of Technology and Education (Grant No.JGY2022-03).

References

[1] Yu B ,Zhou Z ,Yu J , et al.Low-Temperature Performance of Open-Grade Friction Course Based on Computed Tomography Image Reconstruction Technology[J].Journal of Transportation Engineering, Part B: Pavements,2026,152(1).
[2] HE R ,ZHOU N ,ZHANG K , et al.Progress and challenges towards additive manufacturing of SiC ceramic[J].Journal of Advanced Ceramics,2021,10(04):637-674.
[3] Ge X, Wang L, Garcia L J, et al. 3D microstructure reconstruction of heterogeneous material from slice descriptors using explicit neural network[J]. Computer Methods in Applied Mechanics and Engineering, 2026, 448: 118469.
[4] Kyriakou Y, Meyer E, Prell D, Kachelriess M. Empirical beam hardening correction (EBHC) for CT. Med Phys. 2010 Oct;37(10):5179-87.
[5] Dewulf, W.; Tan, Y.; Kiekens, K. Sense and non-sense of beam hardening correction in CT metrology. CIRP Ann. Manuf. Technol.2012, 61, 495–498.
[6] HsinWu T ,Andrew K ,Srinivasan V .Cone-beam breast CT using an offset detector: effect of detector offset and image reconstruction algorithm.[J].Physics in medicine and biology,2022,67(8).
[7] Azevedo S G, Schneberk D J. Calculation of the rotational centers in computed tomography sinograms[J].IEEE Transactions on Nuclear Science, 1990(4):1525-1540.
[8] Donath T, Beckmann F, Schreyer A. Automated determination of the center of rotation in tomography data[J]. Journal of the Optical Society of America A, 2006, 23(5): 1048-1057.
[9] Liu Tong, Malcolm A A. Comparison between fourmethods for central ray determination with wire phan-toms in micro-computedtomography systems[J].Optical Engineering,2006,45(6):066402. (in chinese).
[10] LIU H, CHEN J B, SONG X P, et al. Method for determining the center of rotation based on statistical average[J]. Journal of Test and Measurement Technology, 2019, 33(6): 498-502.
[11] LV Z T, GUI Z G, LlU Y, et al. Industrial CT rotation center calibration method b-ased on weighted average [J]. CT Theory and Applications, 2021,30(5):539-546. (in chinese).
[12] Welkenhuyzen F, Boeckmans B, Tan Y, Kiekens K and Dewulf W. 2014 Investigation of the kinematic system of a 450 kV CT scanner and its influence on dimensional CT metrology applications 5th Conf. on Industrial Computed Tomography (ICT) (Wels, Austria) pp 217–25
[13] LOWE D G .Distinctive Image Features from Scale-Invariant Keypoints[J].Internation-al Journal of Computer Vision, 2004, 60(2):91-110
[14] Hofmann J, Flisch A, Zboray R. Principles for an Implementation of a Complete CT Reconstruction Tool Chain for Arbitrary Sized Data Sets and Its GPU Optimization[J]. Journal of Imaging, 2022, 8(1): 12.
[15] Kingston A, Sakellariou A, Varslot T, Myers G, Sheppard A. Reliable automatic alignment of tomographic projection data by passive auto-focus. Med Phys. 2011 Sep;38(9):4934-45.
[16] Van Aarle W, Palenstijn WJ, Cant J, et al. Fast and flexible X-ray tomography using the ASTRA toolbox. Opt Express. 2016 Oct 31;24(22):25129-25147.